Experimental onset threshold and magnetic pressure pileup for 3D reconnection

[1]T.P. Intrator, X. Sun, [2]G. Lapenta, [1]L. Dorf, [3]I. Furno

Abstract

Magnetic reconnection changes the topology of magnetic field lines to a lower energy state. This process can liberate stored magnetic field energy and accelerate particles during unsteady, explosive events. This is one of the most important processes in astrophysical, space and laboratory plasmas. The abrupt onset and cessation has been a long standing puzzle. We show the first three-dimensional (3D) laboratory example of onset and stagnation of magnetic reconnection between magnetized and parallel current channels (flux ropes) driven by magnetohydrodynamic (MHD) attraction and a 3D plasma current driven instability. Antiparallel magnetic field lines carried by these colliding flux ropes annihilate and drive an electric field. The inflow soon exceeds a threshold for the formation of a reconnection current layer. Magnetic flux and pressure pile up just outside this layer, and eventually become large enough to support MHD back-reaction forces that stall the inflow and stagnate the reconnection process.

PACS 52.35.Vd, 52.30.Cv, 52.35.Bj, 52.30.Ex, 94.30.cp, 94.30.cq

[1] Los Alamos National Laboratory, P-24 Plasma Physics, Los Alamos, New Mexico 87545 USA
[2] Centre for Plasma Astrophysics, Katholieke Universiteit Leuven, Belgium
[3] CRPP-EPFL, Bâtiment PPB, 1015 Lausanne, Switzerland
correspondence should be addressed to TPI, email intrator@lanl.gov

Introduction: For more than half a century it has been realized that a class of processes known variously as magnetic merging, magnetic field annihilation, or magnetic reconnection must be the key to global changes magnetic topology in cosmic solar, magnetosphere and laboratory plasma environments. Energy stored in stressed magnetic fields can produce large scale explosive events that spontaneously evolve due to *unsteady and impulsive* local processes in small volumes of space, and energize particles. For many physical systems of interest, reconnection does not start or proceed in a steady manner, but rather there are unsteady periods of time during which magnetic flux is accumulated, followed rapid energy dissipation events. This situation is inherently three dimensional (3D).

It has become increasingly apparent that magnetic reconnection [1] [2] is important in heliosphere [3], astrophysical [4] and laboratory [5] [6] plasmas. The classic and physically appealing picture of reconnection is the 2D Sweet-Parker [7] [8] type. Plasma that is a nearly perfect electrical conductor entrains anti-parallel magnetic fields. Two mutually approaching, steady flows in the reconnection plane advect these anti-parallel magnetic fields as they collide. An X point forms in the region of closest approach of the magnetic field lines, magnetohydrodynamics (MHD) is locally violated, and according to Ampere's Law the jump in magnetic field induces an out of plane reconnection current in a diffusion region. Reconnection could occur at any or all locations on a line in the out of plane direction, that includes the X point(s).

Recent satellite [9] and laboratory[10] data demonstrate that many situations are 3D. The mutual approach and merging of two or more flux ropes represents the simplest model. Flux ropes [11] [12] [13] are plasma "wires" or current channels that can relax (twist, kink, etc.) and approximately align with a helically twisted magnetic field. Reconnection events often are

impulsive [14] [15], although there is some evidence for quasi-steady-state reconnection in a current sheet between the sun and Earth [16]. Flux ropes can attract each other and merge at a 3D patch, and then sporadic dynamics become an important consideration.

Tremendous efforts have focused on the reconnection rate, usually modeled with asymptotic magnetic fields embedded in steady flows. But little is known regarding the fundamental question: *What causes the onset and termination of reconnection?*

Plasma "wires" with mass respond to MHD forces in 3D: A long experimental history includes toroidal experiments that have created 2D [6] reconnection geometries, along with some "spontaneous" [17] reconnection events. 3D reconnection scenarios [18] have been identified in linear geometries [10] [19]. All these experiments program their magnetic time history and initial conditions using magnet coils that determine the magnetic drive and location of the X-line. However internal forces during magnetic self organization are important for large-scale systems [20]. Here we show a laboratory example of 3D magnetic reconnection where current carrying "wires" that create the magnetic geometry are composed of plasma flux ropes with mass and inertia, are subject to Newton's Law dynamics, and can relax in 3D. Reconnection is impulsively initiated between two freely moving parallel current flux ropes that attract each other, forcing together the oppositely directed magnetic fields between them. As the current in each flux rope ramps up, so does azimuthal magnetic field surrounding each current channel, and therefore the original background axial magnetic field becomes helical. 3D kink instabilities [12][13] grow, which reflect the tendency of flux ropes to align helically with the net magnetic field. Each flux rope collision and flux annihilation region becomes a 3D patch of reconnection.

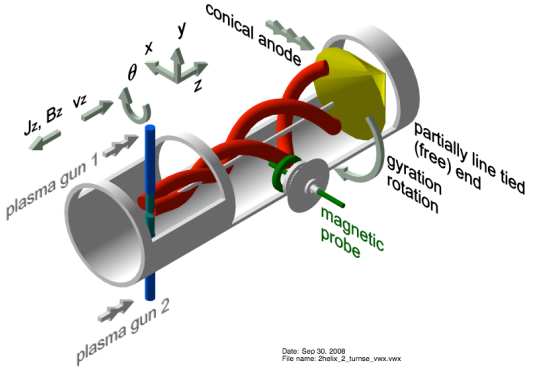

Fig. 1 Schematic of the RSX experiment showing coordinate system and geometry (single arrows), two plasma guns (double arrows) that insert radially but create axial flux ropes, two kinking flux ropes, external conical anode (triple arrow) that allows adjustable axial boundary condition, fiducial line (fictitious and for reference only) at the vessel **z** axis, and magnetic probe inserted through a 3D probe positioner. Radial width is exaggerated x4

Overview of Experimental findings: We experimentally start with a twin flux rope and magnetic island structure [21] [22]. We show a slow inflow threshold for the flux annihilation speed, beyond which there is acceleration culminating in a pileup of magnetic flux accompanied by a change in magnetic topology to a merged reconnected geometry. We then argue that the magnetic field **B** which piles up just outside the reconnection diffusion region interacts with the current density **J** and gives rise to **J**x**B** forces that push back on the merging flux ropes and stagnate the reconnection process. Even though the plasma is moderately collisional, we believe this is a general result because 1) we can distinguish between resistive diffusion and anomalously fast flux annihilation 2) simulations carried out over a range of Lundquist numbers including our experimental values show similar results.

Experiment: A schematic of the Reconnection Scaling Experiment (RSX) [23] is shown in Fig. 1, where we have exaggerated the radial scale and field line pitch by a factor of 4 to highlight the plasma structure. Two plasma guns generate two hydrogen plasma current channels, embedded in a background magnetic guide field $\boldsymbol{B}_{z0}$ = 100 Gauss. Each column has a

current distribution radius *a*~2-3 cm, with an azimuthal magnetic field that vanishes on its axis and radially extends twice this far. The axial boundary condition is an external anode located $L_z \approx 96$ cm from the plasma gun [24]. The guns are fired at time t = 0 and are biased negatively to extract a plasma current $I_p < 0$ from the gun plasma source. The diameter distance between two plasma guns is $L_\perp \sim 6$ cm.

Each flux rope plasma current $I_p(t)$ ramps up during the time interval 1.200-1.220msec for which we show reconnection data. In addition to the mutual attraction of the flux ropes, the kink instability [13] drives each column into two gyrating helices [25] that collide to create 3D merging regions of patchy reconnection, verified by measurements at several nearby axial positions. Meanwhile the current density $\mathbf{J}_z(x,y)$ and magnetic field $\mathbf{B}_\perp = \mathbf{B}_{xy}(x,y)$ distributions evolve as the flux ropes attract each other.

The current channels are emitted from a current source with large impedance relative to the plasma [13]. Rather than following a programmed coil voltage drive, the plasma chooses its own steady voltage bias that is small and time independent. A steady electrostatic axial electric field $\mathbf{E}_{z,es} \approx -1$V/m (±20%) < 0 drives the two flux ropes[13]. The flux rope-to-rope attraction force and velocity can be experimentally increased by increasing the flux rope currents I_p and/or decreasing background guide magnetic field which decreases magnetic compressibility and field line tension restoring force.

As shown in Fig. 1, a magnetic probe with multiple (x-y or x-z) coil pairs spaced at 5mm intervals is placed at θ=180 deg, *z* = 48 cm from the gun in a 3D probe positioner [26] to perform

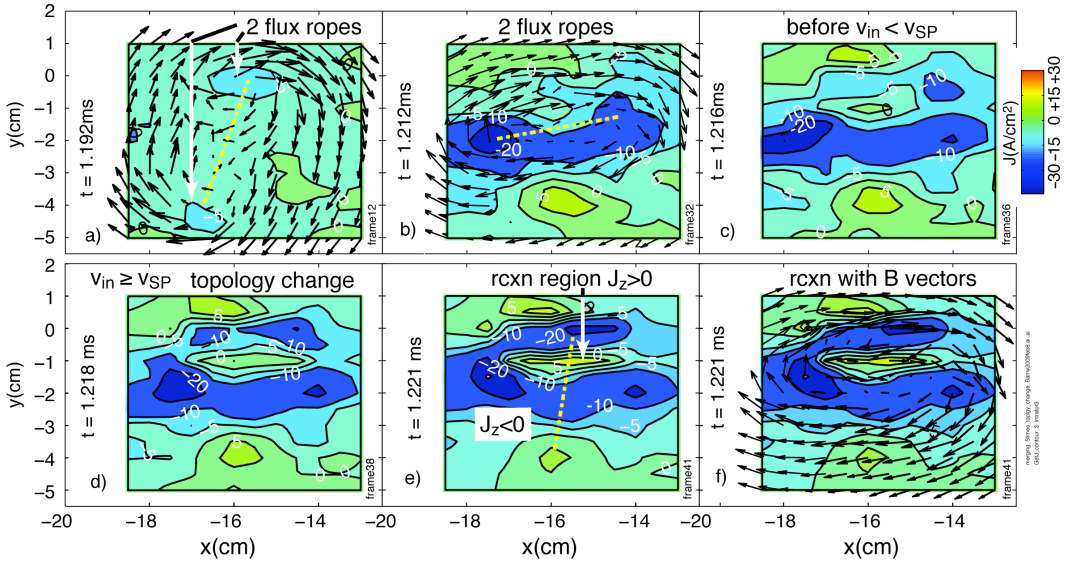

Fig 2 Current density $J_z(x,y)$ derived from magnetic $\mathbf{B}_\perp$ data for $\mathbf{B}_{z0}$=100Gauss in the x-y cutplane at z=48cm, showing contours of calculated $\mathbf{J}_z = \nabla \times \mathbf{B}_\perp / \mu_0$, also corresponding to flux contours. For a) t = 1.192ms the two flux ropes start out vertically aligned, and b) t = 1.212ms shows the cross section line *s* has rotated clockwise, c) t= 1.216ms when v_{in} and flux annihilation rate rise, d) t= 1.218ms when v_{in} exceeds v_{SP} and magnetic topology changes from two flux ropes to a $J_z<0$ region surrounding a $J_z>0$ reconnection region (dashed zero contours). The reconnection rate is maximum at e) t=1.221ms, where the dashed line indicates a cut across the reconnection layer, f) $\mathbf{B}_\perp$ arrow vectors overlaid on $J_z(x,y)$ contours.

a magnetic field profile scan in the x-y cutplane. A triple probe at θ=0 deg, *z* = 48 cm is used to measure the plasma density, pressure, and potential profiles [24] for flux rope and background

plasma. The flux rope density is much greater than the background plasma. Experimental shots are reproducible until the end of the reconnection phase, with many collated shots per data set.

Similar to the reconnection occurring in nature, the merging of flux ropes in RSX is 3D and represents co-helicity, impulsively reconnecting field lines at a small oblique half angle. Since this angle is small and the axial gradient lengths are large compared to the perpendicular gradient lengths, the magnetic flux contours in the two dimensional x-y cutplane still exhibit recognizable 2D coalescing magnetic island geometry. The finite length and non-periodic axial boundary conditions distinguish the RSX reconnection geometry from other toroidal experiments and periodic simulations because 1) axial structure can be important, and 2) the particles neither recirculate periodically nor are constrained to remain near any 2D reconnection plane.

Reconnection Data: Current density $\mathbf{J}_z(x,y)$ derived from magnetic field $\mathbf{B}_\perp < 10$ Gauss data showing reconnection is shown in Fig. 2. Measured vector magnitude and direction of $\boldsymbol{B}_x$ and $\boldsymbol{B}_y$ were used to calculate out of plane current density contours $\mu_0\mathbf{J}_z(x,y;t)=\nabla\times\mathbf{B}_\perp$. Fig. 2a shows two initial flux ropes almost vertically aligned with $\mathbf{J}_z<0$. Fig. 2b shows that the two flux tubes have rotated clockwise about their center of mass, due to the kink motion of individual flux ropes. Triple probe measurements (not shown here) of plasma density, temperature and pressure confirm this rotation. Here each flux rope is fixed at the gun and partially line tied at the other end [12] [27]. Fig. 2c shows $\mathbf{J}_z$ contours when the flux annihilation rate rises from zero. Fig. 2d shows the development of a reconnection region with a reversed current $\mathbf{J}_z>0$ and changed magnetic topology.

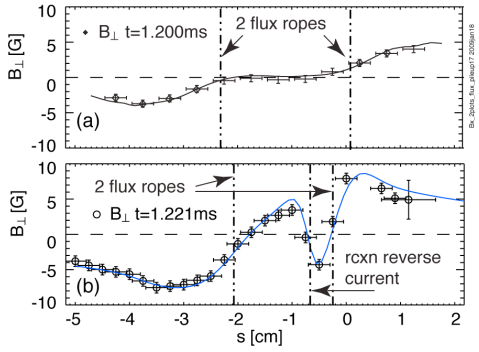

Fig. 3 Magnetic field evaluated on a line *s* that crosses the interaction region between the two colliding flux ropes, (a) before (t=1.200ms) and (b) during (t=1.221ms) reconnection where there is field pile up around the reconnection reversed current region. The curve fits derive from current density $J_z(s)$ with Bennett pinch profiles. Error bars indicate the time averaging period and the measurement uncertainty, and data scatter due to averaging several shots per location.

There is a distorted $\mathbf{J}_z<0$ region that contains the remnants of the original 2 flux ropes surrounding a $\mathbf{J}_z>0$ reconnection region. Reversed currents also exist at the top and bottom in Fig. 2 c-e. Simulations of RSX (see Fig. 19 [28]) suggest this is due to kink motion of separate field lines within each flux rope. Fig. 2e shows the well developed reconnection geometry when the reconnection rate is maximum. Vector $\mathbf{B}_\perp$ arrows are overlaid in Figs. 2a,b,f.

Line cut across reconnection region: As shown in Fig. 3a the initial magnetic field in between the flux ropes is very small. Later in time the flux rope currents gradually ramp up by 50%, but the magnetic field in Fig. 3b increases by a very large factor from a fraction of a Gauss to roughly 5 Gauss. Magnetic flux from transverse $\mathbf{B}_\perp(s)$ piles up as magnetic reconnection develops between t=1.200-1.221 msec. The measured reconnection current $\mathbf{J}_z>0$ (sign reversed from flux rope current) corresponds to an electron diffusion region with radial width > 0.4 cm, which is three times larger than the electron skin depth $c/\omega_{pe} \approx 0.15$cm.

Generalized Ohm's Law: Customarily one estimates reconnection rate and electric field from the time derivative of the vector potential. But since the pileup of magnetic flux and pressure (stagnation) obscure the interpretation of time derivatives, a lower limit is calculated instead. We define the boundary of the reconnection region in the x-y cutplane to be the contour where the current density $\mathbf{J}_z(t)$ changes sign from the $\mathbf{J}_z<0$ flux rope drive to $\mathbf{J}_z>0$ induced

reconnection current. To estimate the axial electric field before and during reconnection, a generalized two fluid and spatial scale Ohm's Law [2] is useful. We evaluate a cutplane average over the reconnection current region. Terms in equation (1) include on the right hand side: 1) anomalous resistivity $\eta_{\|}$* that is expected to be at least as large as the Spitzer value $\eta_{\|}$, 2) electron inertia term total time derivative of the current density $\mathbf{J}_z$, 3) the Hall $\mathbf{J}$x$\mathbf{B}$ term, and 4) divergence of the electron pressure tensor

$$\mathbf{E}_{z,tot} + \mathbf{v}_{in}\mathbf{xB} = \eta_{\|}*\mathbf{J}_z + \mu_0(c^2/\omega_{pe}^2)[\partial/\partial t(\mathbf{J}_z) + \nabla\bullet(\mathbf{vJ} + \mathbf{Jv})] - \mathbf{J}x\mathbf{B}/en - \nabla\bullet\mathbf{P}_e/en] \quad (1)$$

Using the geometry of Fig. 2e we compare each term to $\mathbf{v}_{in}\mathbf{xB}$ to show that anomalous resistivity $\eta_{\|}$* dominates in the electron diffusion region. The diffusion region is larger than the electron skin depth maximum scale size for electron inertia effects [2] [29]. The Hall term includes products $\mathbf{J}_x \times \mathbf{B}_y$ and $\mathbf{J}_y \times \mathbf{B}_x$ associated with ion skin depth c/ω_{pi} length scales where c is the speed of light and ω_{pi} is the ion plasma frequency. These are small near the $\mathbf{J}_z>0$ reconnection current layer where the magnetic field $\mathbf{B}_\perp$ vanishes. The last term contains derivatives $\partial\mathbf{P}_{zx}/\partial x + \partial\mathbf{P}_{yz}/\partial y$ of the electron pressure tensor off diagonal elements. These are important on the hybrid spatial scale of the electron meandering orbit [30] [31] $\lambda_y = (r_{Ge\perp} B_x/B_x')^{1/2}$. We evaluate the electron gyro radius $r_{Ge\perp}$ and scalar magnetic scale length B_x/B_x' where $B_x' = \partial B_x/\partial y$, at the edge of the diffusion region. Our experimental B_{z0}=100Gauss is 10 times larger than necessary to magnetize the meander orbits and reduce the pressure tensor terms. A large guide field $B_{z0} \geq B_x' \lambda_y$ exceeds that of the reconnecting field B_x at the furthest excursion of the bounce motion. For RSX data in Fig 3b $B_x/B_x' \approx 0.4$cm, $r_{Ge\perp} \approx 1.2$cm, $\partial B_x/\partial y \approx$13-14Gauss/cm, $\lambda_y \approx 0.7$cm, $B_x' \lambda_y \approx 10$ Gauss.

Estimate axial electric field: Using Spitzer resistivity ($\eta_{\|}$) we recast equation (1) as the inequality

$$\mathbf{E}_{z,tot} = \mathbf{E}_{z,ind} + \mathbf{E}_{z,es} > \eta_{\|}\mathbf{J}_z - \mathbf{v} \times \mathbf{B} \quad (2)$$

where the total axial electric field is $\mathbf{E}_{z,tot} = \mathbf{E}_{z,ind} + \mathbf{E}_{z,es}$. Electrostatic, time independent $\mathbf{E}_{z,es} < 0$ is measured with a swept Langmuir probe and does not contribute to the inductive reconnection field. Prior to reconnection, the inductive field $\mathbf{E}_{z,ind} = -d\mathbf{A}_z/dt$ is obtained from solutions to a Poisson equation

$$\nabla^2\mathbf{A}_z = \mu_0\mathbf{J}_z = -\nabla x\mathbf{B}_\perp \quad (3)$$

where vector potential is $\mathbf{A} + \nabla\chi$ with gauge $\nabla\chi = -\int E_{z,es}\, dt$, from Fig. 2a-d magnetic data $\mathbf{B}_\perp$. Boundary conditions require that $\mathbf{B}_\perp$ and $\mathbf{A}_z$ vanish for large |x|, |y| > 12cm from the flux ropes.

However evaluation of the laboratory frame time derivative during reconnection is not straightforward because it is small and stagnating [32] at the edge of the reconnection region. This is because flux is lost as fast as it is piling in: to annihilation, outward diffusion, and expulsion of reconnected flux. The total time derivative $d/dt = \partial/\partial t + \mathbf{v}_s\cdot\nabla_s$ includes a negative loss rate and a positive convective inflow, where subscript *s* refers to the line connecting two flux rope centroids (see Figs. 2b, 3). The dash-dot-dot line in Fig. 4a shows that the experimental $d\mathbf{A}_z(t)/dt$ from equation 3 is small. This approach fails to estimate the substantial $\mathbf{E}_z$ that must exist in the laboratory frame during reconnection. Alternatively we use equation 2 and experimental data from Fig. 2 averaged over the reconnection $\mathbf{J}_z>0$ X-point region (where $\mathbf{vxB}$ vanishes). Fig. 4a also displays the lower bound estimates for inductive $\mathbf{E}_{z,ind} = \eta_{\|}\mathbf{J}_z - \mathbf{E}_{z,es}$ (dash-dash line), and total $\mathbf{E}_{z,tot} \geq \eta_{\|}\mathbf{J}_z$ (solid line).

$\mathbf{E}_{z,tot}$ was used to estimate a lower bound for the $\mathbf{E}_z\mathbf{x}\mathbf{B}_\perp$ flux transport inflow speed at the edge of the reconnection region. Fig. 4b shows inflow speed (triangles) evaluated early in time using equivalent current density or flux contours along the line (Fig. 2a,b) labeled *s* which rotates with time, and later in time using $\mathbf{v}_{in}(t) = \mathbf{E}_{z,tot}\mathbf{x}\mathbf{B}_\perp/\mathbf{B}_\perp^2$. Here $\mathbf{B}_\perp$ in the x-y plane is evaluated perpendicular to line *s*.

Threshold for topology change and flux pileup: Even though flux is already being annihilated, flux pileup theoretically initiates when the inflow speed v_{in} delivers flux faster than either resistive diffusion or flux annihilation can process it [4] [33] [21]. In this case v_{in} must exceed the Sweet-Parker speed $v_{SP} = v_A/S^{1/2}$, where $v_A(t)= B_\perp(t)/(\mu_0 n(t) m_i)^{1/2}$ with $B_\perp$ and nm_i evaluated at the $\mathbf{J}_z>0$ diffusion region edge, and Lundquist number $S_\perp = \tau_{D\perp}/\tau_{A\perp}$ is the ratio of resistive diffusion to Alfven transit times. The reconnection flux annihilation rate estimated as v_{in}/v_A in Fig. 4c turns on at t=1.216msec, corresponding to the contours of $\mathbf{J}_z(x,y)$ in Fig. 2c. Several μsec later at t=1.218msec, flux inflow and annihilation rate in Fig. 3b,c have exceeded the Sweet-Parker values. Correspondingly $\mathbf{J}_z(x,y)$ in Fig. 2d exhibits a change in current density (i.e. magnetic) topology. The flux pile up starts when the $\mathbf{J}_z$ topology changes in Fig. 2d as v_{in} exceeds v_{SP}, and several μsec later is easily discerned in Fig. 3b. For larger ratio $B_z/B_\perp$ the inflow speed is slower ($v_{in} < v_{SP}$), no reconnection layer is formed, and the two flux ropes bounce [34].

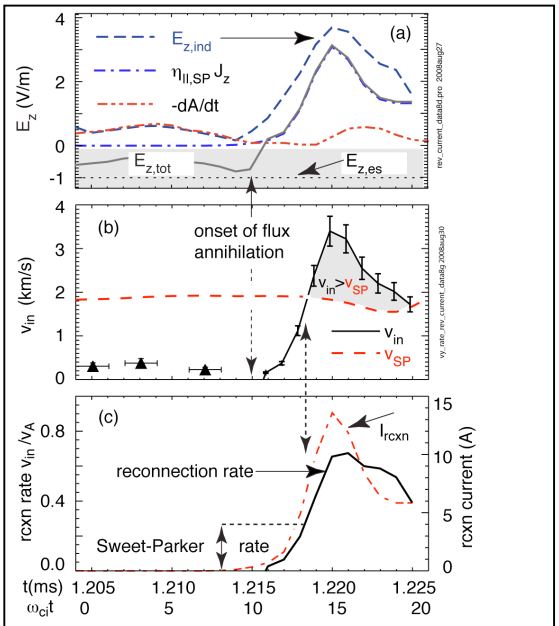

Fig. 4 (a) Estimated lower bound for electric field showing time history of total $E_{z,tot}$, inductive $E_{z,ind}$ measured from time changing flux before stagnation and $\eta_\parallel J_z$ contribution after reconnection is underway, and slowly varying electrostatic $E_{z,es}$ which supports the flux rope current. Flux annihilation commences before the sign of $E_{z,tot}$ changes at t=1.215msec, when the $E_{z,tot}$ field starts to rise. (b) Approach speed of the two flux ropes calculated from flux contours in Figs. 2 (triangles) for early time, and $E_z/B_\perp$ from equation 2 (solid line) for times after 1.215msec, compared with the Sweet-Parker speed. Error bars correspond to averaging time and uncertainty in $B_\perp$ data and calculated J_z. The shaded region corresponds to the time period t> 1.218msec where $v_{in}\geq v_{SP}$. (c) Reconnection rate is shown in along with reconnection reversed current I_p which is an integral measure of the magnetic field line integral around the reconnection region, corresponding to topology change and flux pile up.

Stagnation of reconnection and flux pileup: It is theoretically expected that the magnetic pressure will eventually slow down or stall the merging process [32] [2] [33] [35]. Early in time, the flux rope current data $\mathbf{J}_z(s)$ as shown in Fig. 5a give rise to $\mathbf{J}_z(s)\mathbf{x}\mathbf{B}_\perp(s)$ force densities that initially attract the flux ropes, as seen by the hollow head arrows in Fig. 5b. During reconnection, the reversed current $J_z(s)$ as shown in Fig. 5c and magnetic field pileup give rise to $\mathbf{J}_z(s)\mathbf{x}\mathbf{B}_\perp(s)$ forces that repel the incoming flux ropes as shown in Fig 5d. The double head arrows indicate that the repulsive $\mathbf{J}_z(s)\mathbf{x}\mathbf{B}_\perp(s) \approx$ 30-40N/m^3, at locations s=-1.5, -0.3 cm, are sufficient to stagnate two approaching flux rope momenta with our measured mass density and Fig. 4b estimated mutual inflow speed of 3-4km/sec. Since this repulsion force is at the outside edge of the current sheet, this conclusion is

not affected by possible errors in the pinch current density curve fits to the data inside the reconnection region.

Comparison with computer simulation: The data in Fig. 2 are consistent with a fluid-implicit-particle simulation FLIP3D-MHD. Lagrangian particle interactions computed on a grid and viscous, resistive MHD flow equations [28] [36] allow reconnection to proceed. Movie frames in Fig 6a (before reconnection, $\omega_{ci}t=7$) and Fig. 6b (during reconnection, $\omega_{ci}t=42$), showed similar results for a wide range of Lundquist numbers and system sizes that included experimental RSX parameters shown here. The curled spiral like flux rope shapes in Fig. 6a resemble Figs. 2c,d, and the central reconnection region shape is reminiscent of a Quasi Separatrix Layer [37] [2].

Conclusion: Magnetic reconnection, driven by instability (i.e. waves) and dynamics may couple in a natural way to other wave modes. It is thought that the fast collisionless reconnection rate is increased by dispersive waves with increased phase speed at large wavenumber or small spatial scales [38]. While dispersive whistler and drift waves are predicted to be important for many experiments (e.g. Magnetic Reconnection Experiment [6,10,39]), kinetic Alfvén waves [38] should also relevant for RSX data.

Our data exhibit several experimental features not usually considered in 2D models. The guide field B_{z0} = 100 Gauss is 10 times larger than $\boldsymbol{B}_{\perp}$. For small enough background magnetic field (where $B_{z0} < 100$ Gauss) the flux ropes merge and reconnect, but for larger B_{z0} they bounce. Angular momentum which is usually a robust invariant appears to be important when the two flux ropes orbit each other. These orbits could be an example of a Keplerian central force problem with **J**x**B** attraction force that scales as 1/r and not gravitational $1/r^2$. Other features shown by Figs. 3 and 5 are asymmetric reconnection fields and forces [40] on either side of the reconnection layer. This more likely represents the typical case in nature than ideal and symmetric configurations.

Methods: We describe here some how we carried out the data analyses and the normalization of reconnection time, rate, and speed. RSX [23] coordinates as in Fig. 1 invoke a x-y reconnection ($\perp$) plane, where z is the direction of reconnection current, which differs from solar magnetic coordinates where reconnection is discussed in the x-z plane and y is the out of plane direction. Two plasma guns insert radially and generate two axial hydrogen plasma current channels, embedded in a background magnetic

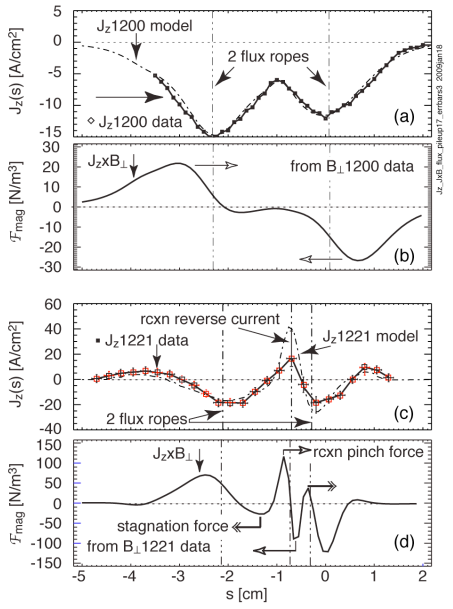

Fig. 5 Current density computed from $\nabla_{\perp}$x$B_{\perp}$, where $B_{\perp}$ in the x-y plane is perpendicular to line *s*, overlaid (a) with the pinch model $J_z(s)$ at time t=1.200ms (before reconnection). The vertical dash-dot-dot lines indicate the fit locations for the flux rope centroids. (b) The J_zx$B_{\perp}$ force densities at t=1.200ms before reconnection, where the hollow head arrows indicate the attraction force. (c) J_z (s) computed from B data overlaid with the pinch model J_z (s) at time t=1.221ms (during reconnection). The vertical dash-dot-dot lines now show 3 magnetic axes. (d) hollow head arrows indicate a pinch force density inside the reconnecting flux rope at y=-0.6 to -0.8cm, and double head arrows show a repelling J_zx$B_{\perp}$ force density back reaction force exerted by the reconnection region upon the incoming flux ropes at s=-1.5cm, -0.3cm.

guide field $\mathbf{B}_{z0}$. The distance between two plasma flux ropes at the plasma guns is $L_\perp \sim 6$ cm. Electron temperature $T_e \approx$ 6-14 eV, plasma density $n \approx$ 1- 3 x 10^{13} cm^{-3}, estimated plasma Spitzer resistivity due to coulomb electron-ion collisions is $\eta_\perp \approx$ 20-25μΩ-m and $\eta_{||} \approx$ 10-12μΩ-m. The mean free path for Coulomb electron-ion collisions using $\eta_\perp$ is approximately 10-20 cm >> $L_\perp$. Each column has a radius corresponding to the current distribution width a~2-3 cm, with a wider magnetic field distribution width, and is terminated at an external anode to length $L_z \approx$ 96 cm [24]. Although we measure a net sonic fluid flow with a Mach probe from gun to anode, we do not consider any axial flow effects on the reconnection. The ion and electron inertial lengths are respectively $c/\omega_{pi} \approx$ 4-5 cm and $c/\omega_{pe} \approx$0.1 cm, where ω_{pi}, ω_{pe}, c are respectively the ion and electron plasma frequencies and the speed of light. In the initial flux ropes, the plasma $\beta_{z0} \approx$30-50%, the axial Alfvén speed referenced to the strong guide field B_{z0}=100 Gauss is $v_{Az} \approx$70km/s. $v_{A\perp} \approx$ 7-8km/s referenced to the $\mathbf{B}_\perp \approx$10 Gauss reconnection field, leading to a Lundquist number $S_\perp = L_\perp v_{A\perp}/(\eta_\perp/\mu_0) = \tau_{D\perp}/\tau_{A\perp} \approx$ 15-20. Here $S_\perp$ is the ratio of resistive diffusion $\tau_{D\perp}$ to Alfvén transit $\tau_{A\perp}$ times in the perpendicular direction, and is used to gauge time and length scales.

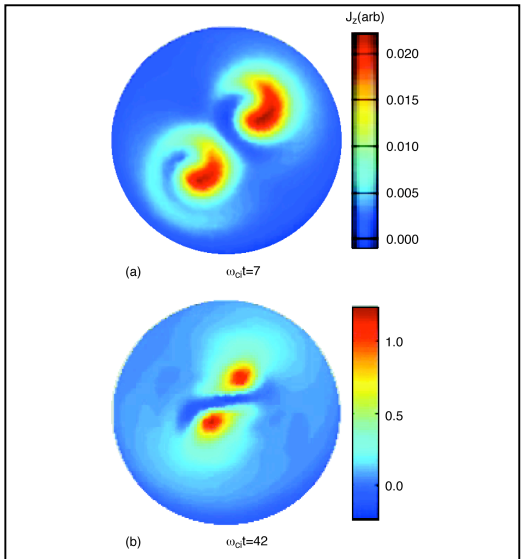

Fig. 6 Computer FLIP3D simulations using a visco-resistive MHD model and realistic boundary conditions of the two RSX flux ropes that mutually attract. Frame (a) shows two flux ropes with $J_z>0$ at $\omega_{ci}t=7$ prior to reconnection. The curling flux rope sections have some similarity to those of Fig. 2c,d. (b) shows more intense J_z at later time $\omega_{ci}t=42$, with an "S" shaped reconnection reversed current $J_z(x,y)<0$ in between the two $J_z>0$ flux ropes.

Similar to the reconnection occurring in nature, the merging of flux ropes in RSX is 3D and represents impulsively reconnecting, co-helicity field lines at a small oblique half angle totaling approximately the flux rope twist (≈ 5deg) plus kink writhe (≈ 0.7deg). In the 2D x-y cutplane picture of reconnection, information can be communicated between locations at the Alfvén speed $v_{A\perp}$which also conveniently normalizes reconnection rate. The Alfvén time is relevant even if ideal, uniform density, bulk waves are cut off. For example a surface Alfvén wave spectrum exists for RSX parameters on the surface of a current carrying column, that includes shear, kink, and compressional modes [41].

Data analyses take advantage of analytic curve fits in Fig 5 for pinch profile current density used by Anderson [32] [2] to model time dependent magnetic flux annihilation in a stagnation flow region. Model flux rope currents plus smaller induced return currents [34] pinch profiles were used. These fits were matched to $\mathbf{J}_z(s)$ data [24], where $J_z(s)=J_{0z}(1+x^2)^{-2}$, $x=(s-s_0)/a$, the flux rope magnetic axis s_0, and $J_z(a)/J_{0z}=1/4$.

Typically the reconnection rate drive by electric field $\mathbf{E}_{z,tot}$, is normalized to inflow speed $\mathbf{v}_{in}= \mathbf{E}_{z,tot}\mathbf{x}\mathbf{B}_\perp/\mathbf{B}_\perp^2$. The total electric field is $\mathbf{E}_{tot} = -\nabla\phi_p - \partial\mathbf{A}/\partial t$,where ϕ_p is the electrostatic scalar potential and $\mathbf{A}$ is the vector potential. We measure ϕ_p with a swept Langmuir probe. It supports a small background, steady state, electrostatic (on the millisecond time scale) $\mathbf{E}_{z,es} = -\nabla\phi_p$ field

that sustains each flux rope (Fig4a). The inductive reconnection electric field $\mathbf{E}_{z,ind}$ is opposite in direction to and overcomes $\mathbf{E}_{z,es}$.

During fast collisionless reconnection, dispersive waves with phase speed proportional to the wavenumber **k** [38] are thought to affect the reconnection outflow geometry and increase the reconnection rate at small scales. Assuming initial $\mathbf{B}=\mathbf{B}_x+\mathbf{B}_{z0}$, growth of $\mathbf{B}_y \approx \mathbf{B}_x$ during reconnection, and $\mathbf{k}=\mathbf{k}_y$, two key dimensionless parameters are the ratio of plasma to magnetic pressure β_k outside the current sheet referenced to $\mathbf{B}_y$ and $\mu_x=(m_e/m_i)(B^2/B_k^2 + \beta_k/2)\approx(m_e/m_i)(1+\beta_{z0}/\beta_k + \beta_k/2)$. These follow from three spatial scales $d_s=d_i(1+v_A^2/c_S^2)^{-1/2}$, $d_e=c/\omega_{pe}$ is the electron skin depth, $d_k=d_i(\mathbf{B}^2/\mathbf{B}_k^2+c_S^2/v_{Ak}^2)^{-1/2}$, where c_S is the ion acoustic sound speed, $d_i=c/\omega_{pi}$ is the ion skin depth, and $v_A=\mathbf{B}^2/(\mu_0 n m_i)^{1/2}$ includes all the **B** components. In this RSX experimental regime $d_i\approx5$cm, $d_e\approx0.17$cm, $d_s\approx0.8$cm, $d_k\approx0.5$cm ≈ diffusion layer size, leading to $\beta_k \approx 40 >> 1$, $\beta_{z0} \approx 0.4$ and $\mu_x \approx 0.06 << 1$. Figure 2 in Rogers et al [38] predicts both whistler and kinetic Alfvén wave effects during the reconnection process.

Acknowledgements: Work supported by Los Alamos Laboratory Directed Research and Development program under LANS Contract No. DE-AC52-06NA25396, and Physics Frontier Center for Magnetic Self Organization in Laboratory and Astrophysical Plasmas, jointly funded by the National Science Foundation and the Department of Energy. We appreciate insightful comments from S.C. Hsu and the reviewers.

Author contributions T.P.I. realized that our data showed 3D instability driven reconnection onset and stagnation and wrote this paper, X.S. acquired most of the data and did substantial data analyses, G.L. carried out computational simulations of the RSX experiment, I.F. and L.D built much of the RSX experiment and discussed the results with T.P.I., X.S. and solidified the arguments and presentation.

References

1. Biskamp D, *Magnetic Reconnection in Plasmas*. Cambridge University Press, Cambridge (2000).
2. Priest ER and Forbes T, *Magnetic Reconnection*. Cambridge University Press, New York (2000).
3. Mozer FS, Phan TD and Bale SD, The complex structure of the reconnecting magnetopause. *Physics of Plasmas* **10**:2480-2485 (2003).
4. Kulsrud RM, *Plasma physics for astrophysics*. Princeton Univ. Press, Princeton, NJ, 08540 (2005).
5. Taylor JB, Relaxation and magnetic reconnection in plasmas. *Reviews of Modern Physics* **58**:741-763 (1986).
6. Yamada M, Review of controlled laboratory experiments on physics of magnetic reconnection. *Journal of Geophysical Research* **104**:14529-14541 (1999).
7. Parker EN, Sweet's mechanism for merging magnetic fields in conducting fluids. *Journal of Geophysical Research* **62**:509-520 (1957).
8. Sweet PA, *The neutral point theory of solar flares*. Cambridge Univ. Press, London, New York (1958).
9. Xiao CJ, Wang XG, Pu ZY, Zhao H, Wang JX, Ma ZW, Gfu SY, Kivelson MG, Liu XZ, Zong QG, Glassmeier KH, Balogh A, Korth A and Reme H, In situ evidence for the structure of a magnetic null in a 3D reconnection event in the Earth's magnetotail. *Nature-Physics* **2**:478-483 (2006).
10. Gekelman W and Pfister H, Experimental observations of the tearing of an electron current sheet. *Physics of Fluids* **31**:2017-2025 (1988).
11. Linton MG, Dynamics of magnetic flux tubes in space and laboratory plasmasa. *Phys Plasmas* **13**:058301 (2006).
12. Furno I, Intrator TP, Ryutov DD, Abbate S, Madziwa-Nussinov T, Light A, Dorf L and Lapenta G, Current-driven rotating-kink mode in a plasma column with a non-line-tied free end. *Physical Review*

Letters **97**:015002-015004 (2006).
13. Sun X, Intrator T.P., Dorf L, Furno I and Lapenta G, Transition of MHD kink stability properties between line-tied and non line tied boundary conditions. *Physical Review Letters* **100**:205004 (2008).
14. Haerendel G, Paschmann G, Sckopke N and Rosenbauer H, The Frontside Boundary Layer of the Magnetosphere and the Problem of Reconnection. *Journ Geophys Res* **83**:3195-3216 (1978).
15. Roederer JG, Global problems in magnetospheric plasma physics and prospects for their solution. *Space Science Reviews* **21**:23-71 (1977).
16. Phan TD, Gosling JT, Davis MS, Skoug RM, Oieroset M, Lin RP, Lepping RP, McComas DJ, Smith CW, Reme H and Balogh A, A magnetic reconnection X-line extending more than 309 Earth radii in the solar wind. *Nature* **439**:175-178 (2006)
17. Egedal J, Fox W, Katz N, Porkolab M, Reim K and Zhang E, Laboratory Observations of Spontaneous Magnetic Reconnection. *Physical Review Letters* **98**:015003 (2007).
18. Baum PJ, Plasma instability at an X-type magnetic neutral point. *Phys Fluids* **16**:1501 (1973).
19. Frank AG, Magnetic reconnection and current sheet formation in 3D magnetic configurations. *Plasma Phys Control Fusion* **41**:A687–A697 (1999).
20. Wan W and Lapenta G, Micro-Macro Coupling in Plasma Self-Organization Processes during Island Coalescence. *Physical Review Letters* **100**:035004 (2008).
21. Biskamp D and Welter H, Coalescence of magnetic islands. *Phys Rev Lett* **44**:1069-1071 (1980).
22. Knoll DA and Chacon L, Coalescence of magnetic islands in the low-resistivity, Hall-MHD regime. *Physical Review Letters* **96**:135001-135004 (2006).
23. Furno I, Intrator T, Torbert E, Carey C, Cash MD, Campbell JK, Fienup WJ, Werley CA, Wurden GA and Fiksel G, Reconnection scaling experiment: a new device for three-dimensional magnetic reconnection studies. *Review of Scientific Instruments* **74**:2324-2331 (2003).
24. Intrator T, Furno I, Ryutov DD, Lapenta G, Dorf L and Sun X, Long lifetime current driven rotating kink modes in a non line-tied plasma column with a free end. *Journal Geophys Res - Space Physics* **112**:A05S90 (2007).
25. Hemsing EW, Furno I and Intrator TP, Fast camera images of flux ropes during plasma relaxation. *IEEE Transactions on Plasma Science* **33**:448-449 (2005).
26. Intrator TP, Sun X, Dorf L, Furno I and Lapenta G, A three dimensional probe positioner. *Review of Scientific Instruments* **79**:10F129 (2008)
27. Ryutov DD, Furno I, Intrator TP, Abbate S and Madziwa-Nussinov T, Phenomenological theory of the kink instability in a slender plasma column. *Physics of Plasmas* **13**:032105 (2006).
28. Lapenta G, Furno I, Intrator T and Delzanno GL, Kink instability of flux ropes anchored at one end and free at the other. *Journ Geophys Res, Space Physics* **111**:A12S06 (2006).
29. Ji H, Ren Y, Yamada M, Dorfman S, Daughton W and Gerhardt S, New insights into dissipation in the electron layer during magnetic reconnection. *Geophys Res Lett* **35**:L13106 (2008).
30. Birn J and Priest ER, *Reconnection of magnetic fields*. Cambridge University Press, New York (2007).
31. Hesse M, Kuznetsova M and Birn J, The role of electron heat flux in guide-field magnetic reconnection. *Physics of Plasmas* **11**:5387-5397 (2004).
32. Anderson C and Priest ER, Time dependent magnetic annhilation at a stagnation point. *Journ Geophys Research* **98**:19395-19407 (1993).
33. Dorelli JC and Birn J, Whistler mediated magnetic reconnection in large systems: Magnetic flux pileup and the formation of thin current sheets. *J Geophys Res* **108**:1133 (2003).
34. Zweibel EG and Rhoads JE, Magnetic merging in colliding flux tubes. *Astrophysical Journal* **440**:407 (1995).
35. Simakov AN, Chacon L and Knoll DA, Semi analytical model for flux pileup limited, dynamically reconnecting systems in resistive magnetohydrodynamics. *Physics of Plasmas* **13**:082103 (2006).
36. Brackbill JU, FLIP MHD: A particle-in-cell method for Magnetohydrodynamics. *Journal of Computational Physics* **96**:163-192 (1991).
37. Milano LJ, Dmitruk P, Mandrini CH and Gomez DO, Quasi separatrix layers in a reduced

magnetohydrodynamic model of a coronal loop. *Astrophysical Journal* **521**:889-897 (1999).
38. Rogers BN, Denton RE, Drake JF and Shay MA, Role of dispersive waves in collisionless magnetic reconnection. *Physical Review Letters* **87**:195004 (2001).
39. Wang Y, Kulsrud R and Ji H, An analytic study of the perpendicularly propagating electromagnetic drift instabilities in the Magnetic Reconnection Experiment. *Physics of Plasmas* **15**:122105 (2008).
40. Mozer FS, Angelopoulos V, Bonnell J, Glassmeier KH and McFadden JP, THEMIS observations of modified Hall fields in asymmetric magnetic field reconnection. *Geophys Res Lett* **35** (2008).
41. Cramer N, F. and Donnelly IJ, Surface and discrete Alfvén waves in a current carrying plasma. *Plasma Phys Control Fusion* **26**:1285-1298 (1984).